Osteoporosis International (2025) 36:917–928
https://doi.org/10.1007/s00198-025-07467-4

ORIGINAL ARTICLE

Simulated low-dose multi-detector computed tomography: spatial effects on surrogate parameters of bone strength at the proximal femur

Nico Sollmann[1,2,3] · Kai Mei[4,5] · Maximilian T. Löffler[2,6] · Sebastian Rühling[2] · Meinrad Beer[1] · Claus Zimmer[2,3] · Jan S. Kirschke[2] · Peter B. Noël[4] · Thomas Baum[2] · Julio Carballido-Gamio[7]

Received: 9 September 2024 / Accepted: 11 March 2025 / Published online: 5 April 2025

Abstract

Summary This study investigated simulated tube current reduction and sparse sampling for low-dose computed tomography (CT) regarding volumetric bone mineral density (vBMD) and cortical bone thickness (Ct.Th) of the proximal femur. Sparse sampling with dose reductions of up to 90% may still allow extraction of bone strength parameters with clinically acceptable accuracy.

Introduction We aimed to investigate effects of CT with simulated lowered tube current and sparse sampling on trabecular and cortical vBMD as well as Ct.Th of the entire proximal femur, its subregions, and with detailed spatial assessments.

Methods Clinical routine multi-detector CT (MDCT) scans covering the hips from 40 patients were used for simulations of low-dose imaging with 50% and 10% of the original tube current (D50, D10) or projections (P50, P10) combined with statistical iterative reconstruction (SIR), which were then compared against original data with full dose (D100 P100) regarding trabecular vBMD, cortical vBMD, and Ct.Th. An automated framework for multi-parametric assessments was used. Relative errors by comparing measures from original data and simulated low-dose data, regression analyses, Bland–Altman analyses, and statistical parametric mapping (SPM, to assess the spatial distribution of accuracy) were computed.

Results Sparse sampling enabled drastic reductions of radiation exposure (down to 10% of original imaging) while still producing determinants of bone strength with clinically acceptable relative changes. Lower biases according to Bland–Altman analyses were observed for sparse sampling compared to imaging with virtually lowered tube currents (D10 P100 versus D100 P10) regarding trabecular vBMD, cortical vBMD, as well as Ct.Th. Better accuracy across the whole proximal femur for D100 P50 than for D50 P100 and for D100 P10 than for D10 P100 was observed.

Conclusions Sparse sampling with SIR may enable drastic reductions of radiation exposure (up to 90% of original doses) for opportunistically measuring image-based surrogate parameters of bone strength.

Keywords Biomechanics · Bone QCT/microCT · Fracture risk assessment · Osteoporosis · Radiology · Screening

✉ Nico Sollmann
nico.sollmann@tum.de

[1] Department of Diagnostic and Interventional Radiology, University Hospital Ulm, Ulm, Germany

[2] Department of Diagnostic and Interventional Neuroradiology, School of Medicine and Health, TUM Klinikum Rechts der Isar, Technical University of Munich, Munich, Germany

[3] TUM-Neuroimaging Center, TUM Klinikum Rechts der Isar, Technical University of Munich, Munich, Germany

[4] Department of Radiology, Perelman School of Medicine, University of Pennsylvania, Philadelphia, PA, USA

[5] Department of Diagnostic and Interventional Radiology, School of Medicine and Health, TUM Klinikum Rechts der Isar, Technical University of Munich, Munich, Germany

[6] Department of Diagnostic and Interventional Radiology, University Medical Center Freiburg, Freiburg, Germany

[7] Department of Radiology, University of Colorado – Anschutz Medical Campus, Aurora, CO, USA

Introduction

Osteoporosis is globally highly prevalent and characterized by low bone mass and micro-architectural deterioration, predisposing mostly older individuals to fragility fractures [1]. Fractures can affect multiple regions of the body, but hip fractures are the second most common ones following vertebral fractures and entail high morbidity and mortality, thus making up a high socio-economic burden [1]. To diagnose osteoporosis and assess the individual fracture risk, imaging methods including dual-energy X-ray absorptiometry (DXA) and quantitative computed tomography (CT) are used in clinical routine [2–5]. While DXA represents the widely used reference standard technique for bone densitometry by measuring areal bone mineral density (aBMD), quantitative CT is an alternative that generates three-dimensional (3D) datasets enabling volumetric BMD (vBMD) assessments [2, 3, 5].

The 3D nature of a CT dataset provides the opportunity to perform more advanced analyses beyond extraction of vBMD [2, 4]. This is of high clinical importance as a patient's susceptibility to fragility fractures cannot solely be explained by decreased vBMD, because bone strength and resistance to fractures are also determined by other parameters such as bone geometry and microstructure with different contributions from the trabecular and cortical bone compartments [6–8]. To date, the multi-parametric capability of CT at the proximal femur has been extended beyond vBMD calculations to estimates of bone strength with finite element modeling (FEM) [9], dedicated measurements of cortical bone thickness (Ct.Th) [10], as well as to statistical models of shape and imaging features [11], and to localized parametric comparisons using computational anatomy approaches such as statistical parametric mapping (SPM) [10, 12–14]. While those approaches including underlying segmentations of the proximal femur are oftentimes performed in isolation and are labor-intensive, an automated framework to perform multi-parametric assessments of the proximal femur with extraction of major determinants of bone strength has been introduced [10].

However, quantitative CT for diagnosing osteoporosis and assessing the individual fracture risk comes at the cost of higher radiation exposure to the scanned patient when compared to DXA, which becomes even more relevant in the common clinical scenario when multiple measurements are needed due to reevaluation purposes or therapy monitoring [2–4, 15]. Consequently, strategies to reduce radiation exposure from imaging and increase patient safety are highly desirable but need to be carefully balanced against sufficiently high image quality and accuracy of CT-derived measures [16, 17]. Reductions of radiation dose can be established, among other options, with systematically lowered tube current or by acquisitions of fewer projections during scanning, which is referred to as sparse sampling [18–23]. When brought together with advanced image reconstruction algorithms such as statistical iterative reconstruction (SIR), considerable radiation dose reductions may become feasible while assuring sufficient image quality [18–20, 24]. In this context, it has been shown that the application of sparse sampling with SIR to multi-detector CT (MDCT) images with a reduction down to 10% of original projections may still produce robust integral (cortical + trabecular) vBMD values with small and clinically acceptable bias (e.g., + 6 mg/cm^3) compared to full-dose imaging for measurements at the femoral neck [25]. On a similar note, a radiation dose reduction of 50% through sparse sampling with SIR may be established for FEM-based estimation of femoral failure load [20]. However, it has not been investigated to date whether and to what level strategies for radiation dose reduction may be applied in keeping with the requirement of accurately delivering major determinants of bone strength (i.e., vBMD and Ct.Th) when considering the entire proximal femur, its compartments (trabecular and cortical), and its subregions at multiple scales.

Against this background, the hypothesis of this study was that sparse sampling with SIR applied to MDCT of the proximal femur allows for reductions of radiation exposure of 50% or more, while still producing accurate determinants of bone strength across the whole proximal femur. Therefore, we aimed to assess the independent effects of both sparse sampling and tube current reductions with SIR on MDCT-based calculations of Ct.Th and cortical and trabecular vBMD in the total proximal femur, in three of its subregions (femoral head, femoral neck, and trochanteric region), and at a local level using the SPM framework.

Methods

Study design and participants

This retrospective single-site study was approved by the local institutional review board (registration number 5022/11-A1) and conducted in accordance with the Declaration of Helsinki. The requirement for written informed consent was waived due to the retrospective study design.

Patients above the age of 50 years who had undergone thoraco-abdominal MDCT during clinical routine and following clinical indications were included and identified by searching our institutional Picture Archiving and Communication System (PACS). The exclusion criteria were (1) any known history of malignant bone lesions (such as bone metastases or primary bone cancer), (2) hematological

disorders, (3) any history of proximal femur fractures, (4) presence of hip endoprostheses, and (5) any known metabolic bone disorders aside from osteoporosis. In total, 40 subjects were included (26 males and 14 females, mean age ± standard deviation [SD] 69.1 ± 10.0 years). This cohort (except for one patient, who was excluded due to image processing issues) has been previously investigated to determine the effects of methods for radiation dose reduction on integral vBMD measurements at the femoral neck [25]. In brief, this previous study used simulated low-dose scans by lowering tube currents and applying sparse sampling, and integral vBMD values were then compared between different dose levels, numbers of projections, and image reconstruction approaches [25]. Application of sparse sampling with a reduction down to 10% of projections of original scans delivered robust values, with clinically acceptable relative changes [25]. Hence, this previous study did not investigate other parameters beyond integral vBMD, did not investigate the entire proximal femur together with its subregions, and did not provide detailed spatial assessments [25].

Imaging by multi-detector computed tomography

All MDCT scans were performed during clinical routine and due to clinical indications (e.g., oncological staging) in one tertiary care center (academic medical center). None of the patients provided more than one MDCT dataset to the present study (i.e., 40 scans from 40 different patients retrospectively included). Scanning by MDCT covered the proximal femur of both sides at least down to the lesser trochanter in all subjects [25]. Imaging was performed with a 256-row MDCT scanner (iCT; Philips Healthcare, Best, The Netherlands) and with a standard reference phantom (Mindways Osteoporosis Phantom; Austin, TX, USA) that was placed beneath the patients for calibration purposes. Tube voltage and rotation time were 120 kVp and 0.4 s, the pitch ranged from 0.59 to 0.91, and the overall maximum tube current during the thoraco-abdominal scans ranged from 200 to 400 mA (exact tube current implicitly modulated by the scanner, tube current at the proximal femur ranging between approximately 100 and 200 mA) [25]. The imaging examinations were performed after the administration of an intravenous contrast agent (Imeron 400; Bracco, Konstanz, Germany) using a high-pressure injector (Fresenius Pilot C; Fresenius Kabi, Bad Homburg, Germany) and considering a delay of 70 s, a flow rate of 3 mL/s, and an individual body weight-dependent dose (i.e., 80 mL for body weight < 80 kg, 90 mL for body weight between 80 and 100 kg, 100 mL for body weight > 100 kg). In addition, all patients drank approximately 1000 mL of an oral contrast agent (Barilux Scan; Sanochemia Diagnostics, Neuss, Germany) over a period of about 1 h prior to scanning. The effective dose of MDCT scans ranged between approximately 3.6 and 9.1 mSv [25].

Image data analysis

Low-dose simulations and statistical iterative reconstruction Low-dose scans were simulated by using (1) virtual tube current reduction and (2) sparse sampling in all patients using in-house developed scripts. The simulation algorithm to generate lower tube currents for MDCT scans was based on raw projection data, and MDCT system parameters were known to take the electronic noise into account [18, 19, 21, 22, 25, 26]. Furthermore, the raw imaging data of the examinations were exported directly from the MDCT system and used for simulations of sparse-sampled imaging. For sparse sampling, the number of projections per full rotation was systematically reduced, while other parameters (e.g., projection geometry and subject location) were kept the same [18, 19, 21, 22, 25, 27].

For both virtually lowered tube current and sparse sampling, a stepwise approach was followed, generating low-dose simulations at 50% and 10% of the original tube current (D50, D10) and at 50% and 10% of the original projection data for sparse sampling (P50, P10) by reading only every second or tenth projection angle and deleting the remaining projections in the sinogram. The original MDCT imaging data with 100% tube current and 100% projections (i.e., original full-dose images) were defined as D100 P100.

The full-dose and dose-reduced simulated images were reconstructed with an in-house developed SIR algorithm [18–20]. We applied ordered-subset separable paraboloidal surrogation and a momentum-based accelerating approach for SIR [28]. A proper regularization was used for SIR to optimize the image quality for virtual low-dose scans. To enhance convergence and to further depress image noise while achieving adequate bone/soft tissue contrast, a regularization term based on a Huber penalty was applied, with the distinct strength of the regularization term being selected in consensus with three board-certified radiologists (aiming at visually high diagnostic image quality). The voxel intensities (mass attenuation coefficients, m^2/kg) were calibrated to Hounsfield units (HU) by using air/water information from the MDCT calibration data.

Extraction of determinants of bone strength To derive cortical and trabecular image-based determinants of bone strength from the full-dose and dose-reduced simulated images, an automated image analysis pipeline was applied (to left and right periosteal proximal femoral segmentations) [10]. Briefly, cortical bone was segmented using a non-local fuzzy c-means algorithm where the vBMD and the distances of each bone voxel to the closest soft tissue voxel were used as clustering features. Surface-based Ct.Th maps were then generated using the streamline integral thickness (SIT) technique, which takes into account partial volume effects. To perform subregional analyses at corresponding

anatomical subregions across all scans in the study (full-dose and dose-reduced scans), volumes and surfaces of interest (femoral head, femoral neck, and trochanteric region) were predefined in a femoral template (Fig. 1) and transferred to all scans using affine and non-linear image registrations based on shape. Similarly, maps of vBMD and Ct.Th were spatially normalized to a femoral template using affine and non-linear registrations of the femoral shapes to perform localized volume-based and surface-based analyses using the SPM framework [10, 29]. We calculated integral vBMD (in mg/cm^3) for the total hip; cortical vBMD (in mg/cm^3) for the femoral neck and trochanteric region; trabecular vBMD (in mg/cm^3) for the femoral head, femoral neck, and trochanteric region; and Ct.Th (in mm) for the femoral neck and trochanteric region. Cortical bone at the femoral head was not analyzed due to its thinness.

All parameters were computed for both the left and right hips for the full-dose data (D100 P100) as well as for the simulated low-dose data of all levels (D50 P100, D10 P100 and D100 P50, D100 P10). The reproducibility values of compartmental vBMD and Ct.Th calculations for this automated pipeline in test–retest analyses have been reported to range under a root mean square coefficient of variation (CV_{RMS}) of 1.7% (absolute precision error = 1.53 mg/cm^3) and 2.7% (absolute precision error = 0.042 mm), respectively.

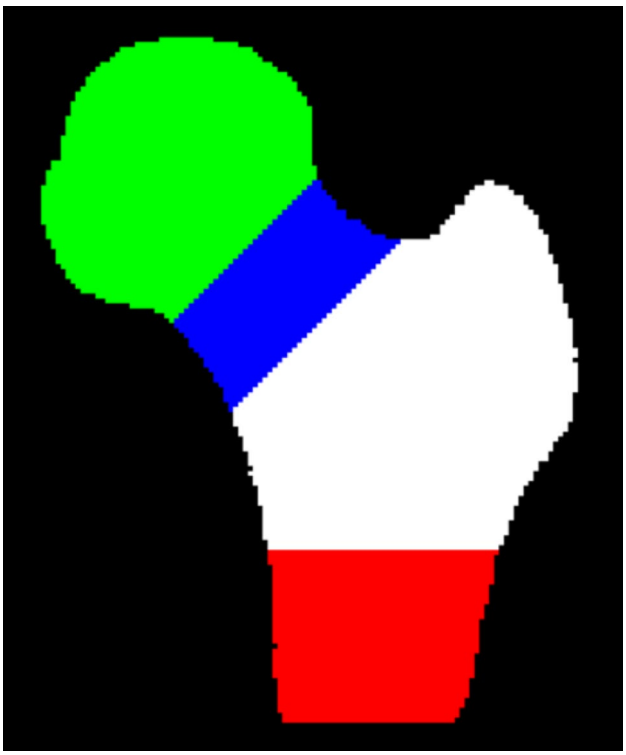

Fig. 1 Coronal cross-section of the proximal femoral template showing the femoral head (green), femoral neck (blue), and trochanteric (white) regions of interest used in the analyses of this study

Moreover, the reproducibility for local Ct.Th calculations has been reported to vary spatially across the proximal femur (CV_{RMS} better than 7% with absolute precision errors smaller than 0.07 mm, excluding the femoral head) [10]. Analyses were performed independently for the left and right femur.

Statistical analysis Statistical data analyses were performed with GraphPad Prism (version 10.1.1.; GraphPad Software, Boston, MA, USA) and MATLAB (version R2022b; The Mathworks Inc., Natick, MA, USA).

Descriptive statistics were calculated for all measures, including mean, SD, median, minimum, and maximum values, considering full-dose data (D100 P100) as well as the simulated low-dose data of all levels (D50 P100, D10 P100 and D100 P50, D100 P10). Shapiro–Wilk tests indicated a normal distribution for the quantitative data. Trabecular vBMD, cortical vBMD, and Ct.Th values for the femoral neck of both sides were used to create boxplots. To assess the accuracy of the low-dose bone parameters, we performed linear regression and Bland–Altman analyses with respect to the full-dose parameters. We also calculated relative differences for the low-dose data in relation to the full-dose MDCT data (in %) and used paired *t*-tests to compare relative differences between D50 P100 and D100 P50 and between D10 P100 and D100 P10 data. Differences were considered statistically significant at a p-value < 0.05.

We used the SPM framework to assess the spatial distribution of the accuracy of low-dose vBMD and Ct.Th values on a voxel-by-voxel and vertex-by-vertex basis, respectively, yielding maps of parameters derived from linear regression analyses.

Results

Sparse sampling, virtual tube current reduction, and calculation of determinants of bone strength using the automated pipeline were successfully achieved in all included scans. Table 1 summarizes the subregional measures and relative differences for trabecular and cortical vBMD as well as for Ct.Th for the left and right hips depending on the level of tube current lowering or sparse sampling. Table 1 also indicates which of the relative differences were significantly different between the data with simulated lowered tube currents and sparse sampling. The distributions of the trabecular vBMD, cortical vBMD, and Ct.Th data for the femoral neck of both the left and right proximal femora are summarized in Fig. 2 with box plots.

Overall, trabecular vBMD for the three subregions (femoral head, neck, and trochanteric region) decreased with virtual lowering of 50% of the tube current, with relative differences between − 3.1% and − 0.5%, while it increased

Table 1 Trabecular and cortical volumetric bone mineral density (vBMD) and cortical bone thickness (Ct.Th) from subregional analyses at the left and right proximal femur

		D100 P100	D50 P100	Δ %	D10 P100	Δ %	D100 P50	Δ %	D100 P10	Δ %
Left proximal femur										
Integral vBMD	**Total hip**	200.9 ± 44.1	208.0 ± 46.3	3.5	310.9 ± 75.1	54.7**	204.5 ± 44.3	1.8	203.9 ± 44.3	1.5
Trabecular vBMD	**Head**	144.9 ± 31.2	142.2 ± 40.0	− 1.9	163.3 ± 25.7	12.7**	143.9 ± 33.8	− 0.6	127.7 ± 47.0	− 11.8
	Neck	75.4 ± 46.7	73.2 ± 53.1	− 2.9	119.1 ± 45.3	57.9	76.1 ± 49.1	0.9	60.8 ± 66.9	− 19.3
	Trochanter	57.7 ± 38.5	55.9 ± 44.7	− 3.1	107.8 ± 36.6	86.7	57.7 ± 43.1	− 0.1	44.8 ± 62.0	− 22.4
Cortical vBMD	**Neck**	637.6 ± 39.5	648.5 ± 65.7	1.7	790.2 ± 113.6	23.9**	649.6 ± 44.7	1.9	665.1 ± 73.3	4.3
	Trochanter	639.0 ± 34.6	653.4 ± 63.6	2.3	793.6 ± 103.7	24.2**	651.2 ± 40.9	1.9	666.6 ± 72.3	4.3
Ct.Th	**Neck**	1.46 ± 0.25	1.50 ± 0.24	2.3*	1.69 ± 0.24	15.7**	1.44 ± 0.24	− 1.6	1.46 ± 0.23	− 0.2
	Trochanter	1.67 ± 0.29	1.70 ± 0.27	1.4*	1.81 ± 0.27	8.1**	1.66 ± 0.27	− 1.1	1.66 ± 0.26	− 0.6
Right proximal femur										
Integral vBMD	**Total hip**	205.5 ± 44.0	213.1 ± 45.6	3.7*	309.7 ± 73.3	50.7**	208.1 ± 44.6	1.3	207.4 ± 44.7	1.0
Trabecular vBMD	**Head**	150.6 ± 32.0	148.1 ± 39.9	− 1.7	167.1 ± 27.3	11.0	148.5 ± 34.8	− 1.4	133.1 ± 43.6	− 11.6 + +
	Neck	76.6 ± 45.5	75.5 ± 49.7	− 1.4	120.2 ± 47.9	56.9	76.0 ± 48.8	− 0.8	63.1 ± 57.8	− 17.7
	Trochanter	57.8 ± 39.5	57.5 ± 43.9	− 0.5	108.8 ± 41.1	88.1	58.1 ± 43.4	0.4	46.1 ± 57.0	− 20.3
Cortical vBMD	**Neck**	638.8 ± 37.1	649.2 ± 64.3	1.6	768.5 ± 106.4	20.3**	649.6 ± 41.9	1.7	661.5 ± 59.5	3.6
	Trochanter	640.2 ± 34.0	654.7 ± 62.9	2.3	779.9 ± 112.1	21.8**	652.7 ± 39.7	2.0	665.5 ± 65.2	4.0
Ct.Th	**Neck**	1.51 ± 0.21	1.54 ± 0.20	2.1*	1.73 ± 0.24	14.8**	1.48 ± 0.20	− 2.1	1.50 ± 0.19	− 0.80
	Trochanter	1.75 ± 0.23	1.77 ± 0.22	1.3	1.89 ± 0.22	7.9**	1.72 ± 0.22	− 1.7 +	1.73 ± 0.20	− 1.3

This table shows mean ± standard deviation (SD) values for integral total hip vBMD; trabecular vBMD of the femoral head, femoral neck, and trochanteric region; cortical vBMD of the femoral neck and trochanteric region; and for Ct.Th of the femoral neck and trochanteric region. Data are shown for the full-dose (D100 P100) as well as for the virtually lowered tube current (D50 P100, D10 P100) and sparse-sampled (D100 P50, D100 P10) scans. Relative differences (in %, Δ %) are shown for comparisons of respective values against the original data.

*Significantly larger relative differences compared to D100 P50 / + Significantly larger relative differences compared to D50 P100.

**Significantly larger relative differences compared to D100 P10 / ++ Significantly larger relative differences compared to D10 P100.

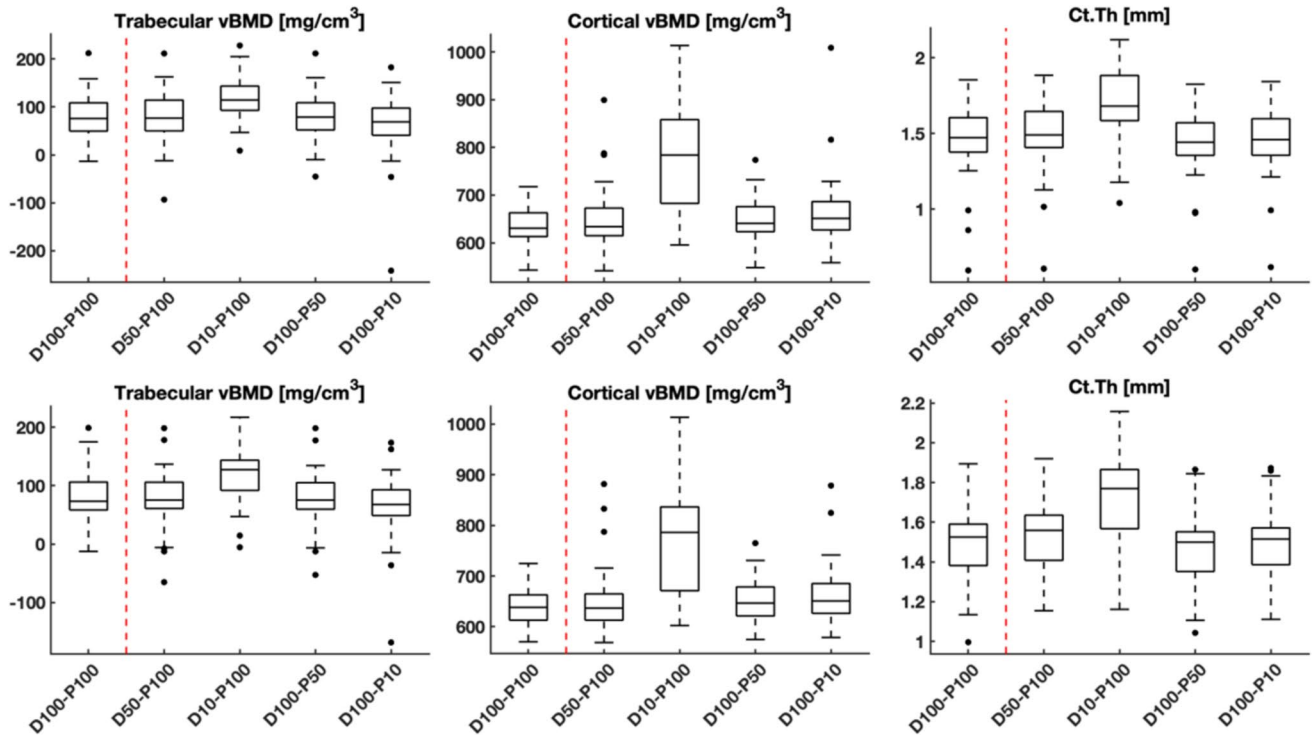

Fig. 2 Trabecular and cortical volumetric bone mineral density (vBMD) and cortical bone thickness (Ct.Th) for the femoral neck. Box plots with 10–90 percentile whiskers (and data points outside of those ranges displayed as single points) are shown for trabecular vBMD, cortical vBMD, and Ct.Th for the left (top) and right (bottom) femoral necks. Data from original scans (D100 P100) and from scans simulated with lowered tube current (D50 P100, D10 P100) and using sparse sampling (D100 P50, D100 P10) are shown

with virtual lowering of the tube current down to 10% of the full-dose data with relative differences between 11% and 88.1% (Table 1). On the other hand, sparse sampling decreased trabecular vBMD up to − 1.4% for D100 P50 and up to − 22.4% for D100 P10, except for the left femoral neck (0.9%) and right trochanteric region (0.4%) at D100 P50. While no significant differences were found between relative differences of D50 P100 and D100 P50 for trabecular vBMD, small significant differences were observed regarding relative differences of D10 P100 and D100 P10 for trabecular vBMD at the femoral head (Table 1).

Dose reduction strategies overestimated cortical vBMD with significantly larger relative differences for D10 P100 than D100 P10, while virtual lowering of the tube current and sparse sampling overestimated and underestimated Ct.Th, respectively. For most comparisons, virtual lowering of the tube current consistently yielded larger relative differences than sparse sampling (Table 1).

Slopes (m), intercepts (b), and R^2 values of the regression analyses, and limits of agreement (LOA) and number of scans out of the LOA of the Bland–Altman analyses explaining the accuracy of the low-dose parameters are shown in Supplementary Tables 1 and 2. Specifically, D50 P100 and D100 P50 performed better for total hip integral vBMD ($m = 1.006$, $R^2 = 0.916$ and $m = 1.004$, $R^2 = 0.999$, respectively) and worst for cortical vBMD at the trochanteric region ($m = 1.395$, $R^2 = 0.570$ and $m = 1.108$, $R^2 = 0.877$, respectively). On average, the slopes were 1.107 and 1.031 for D50 P100 and D100 P50, respectively. The average slopes for D10 P100 and D100 P10 were 1.221 and 1.072, respectively, ranging from 0.952 to 2.496 and 1.004 to 1.409. With respect to the Bland–Altman analyses, most of the LOA were larger and more scans were out of the LOA for simulations of tube current reductions compared to sparse sampling (Supplementary Tables 1 and 2). Plots of the regression and Bland–Altman analyses are shown in the Supplementary Figs. 1 to 6.

Figures 3, 4, and 5 summarize the results from the SPM framework as maps of slopes and R^2 values from linear regression analyses for vBMD and Ct.Th, showing better accuracy across the whole proximal femora for D100 P50 than for D50 P100 and for D100 P10 than for D10 P100.

Discussion

This study systematically investigated the effects of low-dose MDCT by means of virtual tube current reductions and sparse sampling for trabecular and cortical vBMD as well as Ct.Th at the proximal femur. As hypothesized, sparse

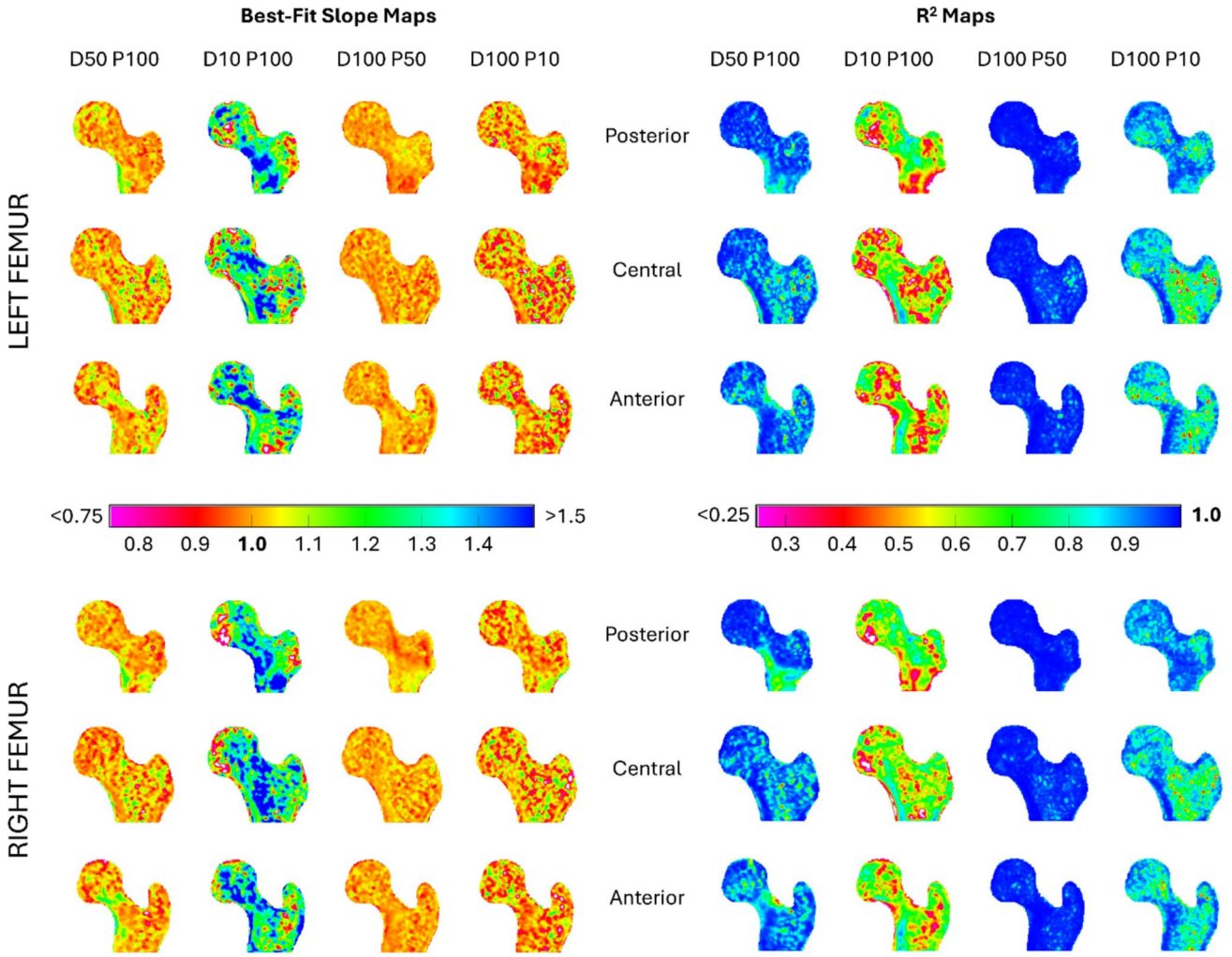

Fig. 3 Voxel-wise analyses of the accuracy of low-dose volumetric bone mineral density (vBMD) of the proximal femur. Coronal cross-sections (posterior, central, and anterior) for the left femur (top section) and right femur (bottom section) showing the best-fit slope maps and R^2 maps of the voxel-wise linear regressions between the original scans (D100 P100) and scans simulated with lowered tube current (D50 P100, D10 P100) and using sparse sampling (D100 P50, D100 P10)

sampling with SIR applied to MDCT of the proximal femur enabled drastic reductions of radiation exposure (down to 10% of original imaging data) while still producing determinants of bone strength with clinically acceptable relative changes at different scales including the full proximal femur, three of its most common subregions, and locally at the voxel and vertex levels.

Given the rather small relative changes of trabecular and cortical vBMD as well as Ct.Th when MDCT data were simulated with sparse sampling and SIR, it seems realistic to perform low-dose imaging with a radiation dose of as low as 10% of the original setup. This finding may be of particular relevance for patient safety given the "As Low As Reasonably Achievable" (ALARA) principle that demands imaging with the minimum radiation dose that still leads to images with diagnostic quality [30]. Beneficial safety effects of low-dose MDCT may accumulate, given that a high proportion of patients undergoes repeated imaging for reevaluation purposes or therapy monitoring [2–4, 15]. Not only is osteoporosis common in the elderly and particularly in postmenopausal women, but also malignant diseases and chemotherapy against many cancers can cause bone loss even in younger patients, making follow-up imaging exams over time necessary as anti-osteoporotic drugs may take effect differently between individuals [31–33].

In agreement with our current findings, a previous study has proposed that sparse sampling with SIR applied to MDCT images of the proximal femur with a reduction down to 10% of original projections may still produce robust vBMD values as compared to full-dose imaging [25]. However, in this previous study, vBMD was only derived from representative focal regions of interest manually placed at

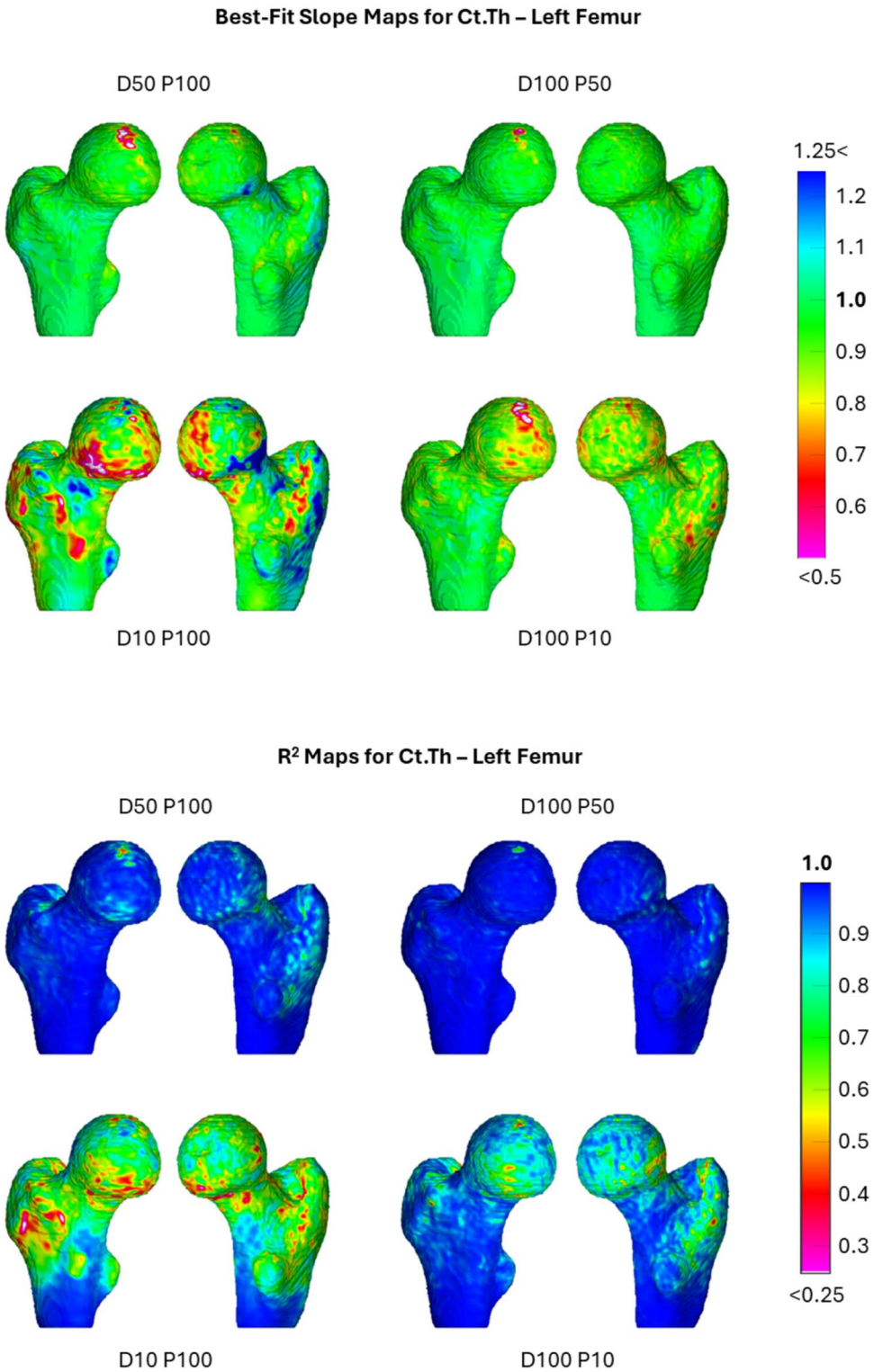

Fig. 4 Vertex-wise analyses of the accuracy of low-dose cortical bone thickness (Ct. Th) of the left proximal femur. Surface representations of best-fit slope maps and R^2 maps of the vertex-wise linear regressions between the original scans (D100 P100) and scans simulated with lowered tube current (D50 P100, D10 P100) and using sparse sampling (D100 P50, D100 P10)

the femoral neck, and only integral vBMD was considered [25]. Yet, advanced image analysis pipelines may overcome the labor-intensive segmentation steps by automatization of volumetric segmentations of subregions or entire volumes of a structure, and could facilitate full exploitation of the 3D datasets MDCT can deliver as an effort to output multiparametric determinants of bone strength [10, 11, 29]. While assessments of aBMD or vBMD are widely performed and remain the standard for diagnosing osteoporosis and for evaluating individual fracture risk, it is known that those

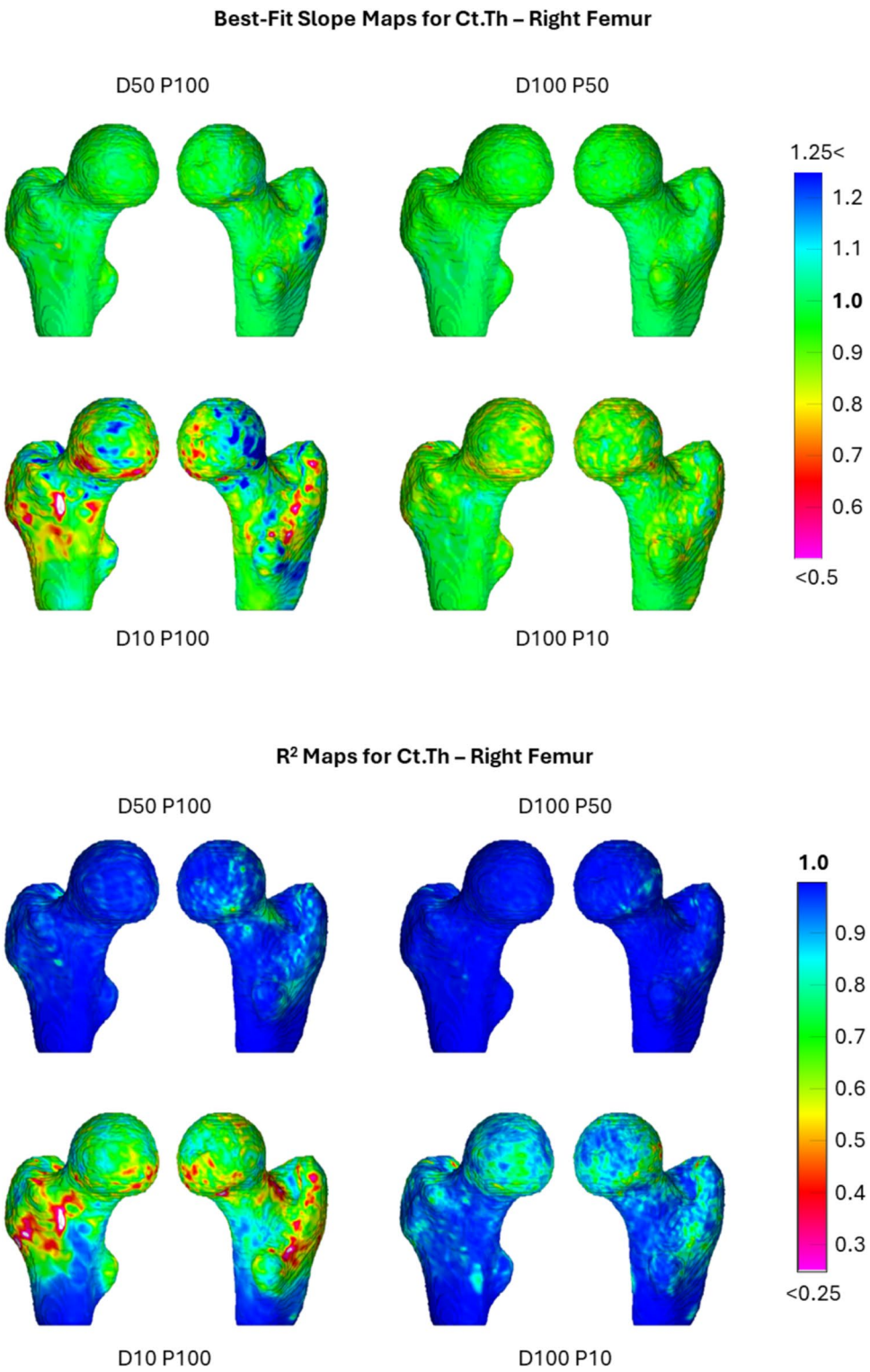

Fig. 5 Vertex-wise analyses of the accuracy of low-dose cortical bone thickness (Ct.Th) of the right proximal femur. Surface representations of best-fit slope maps and R^2 maps of the vertex-wise linear regressions between the original scans (D100 P100) and scans simulated with lowered tube current (D50 P100, D10 P100) and using sparse sampling (D100 P50, D100 P10)

parameters alone may not be able to explain individual susceptibility to fragility fractures and bone strength [6–8]. For instance, it has previously been suggested that DXA-based aBMD values only account for about 60 to 70% of the variation in bone strength [6]. Regarding Ct.Th as analyzed in the present study, the anatomical distribution of cortical bone especially in the proximal femoral metaphysis in older individuals is a critical component for determining resistance to hip fractures, with trabecular bone probably even playing a lesser role in this context [34, 35]. Specifically, at the proximal femur, compressive cracks of cortical bone of superior parts of the trochanter and femoral neck oftentimes reflect

the initiation of hip fractures [36, 37]. Hence, especially in the light of resistance against imminent hip fractures, low-dose imaging needs to be able to also correctly capture Ct.Th as a parameter beyond vBMD.

While our results for sparse sampling are encouraging, commercially available CT systems do not provide the option of this approach, but prototype solutions have been concepted in the past. In contrast, any reductions of tube current can be easily established with conventional MDCT scanners, and particularly photon-counting CT that becomes increasingly available shows high potential for dose reductions [38, 39]. While the results of this study indicate that sparse sampling may facilitate more drastic reductions of radiation dose (down to 10% of original imaging), lowering tube currents by at least 50% could still enable imaging that can produce determinants of bone strength with clinically acceptable accuracy. This may partly be due to the reconstruction approach of SIR, as it may be capable of compensating for streaking artifacts and noise, amongst other advantages over conventional filtered back projection [24]. However, with current MDCT hardware and commonly used energy-integrating detectors, noise is likely to severely increase when there are not statistically enough X-ray photons reaching the detector, leading to high electronic noise [40]. This might be the leading cause why considerable changes of trabecular and cortical vBMD as well as Ct.Th measurements occurred for the reduction down to 10% of the original tube current. In the practical setting, the change of measures with lowering of tube currents may be associated with changes of the energy spectrum reaching the detector or perhaps with non-linearity of detectors for widely used MDCT scanners, which may be circumvented by photon-counting CT scanners [41]. However, our findings stemming from simulations may not necessarily be observed on the same scale in clinical practice. Yet, in vivo validations apparently cannot be established as repeated MDCT scanning with varying settings is prohibited due to accumulating radiation exposures to the patient. An alternative could be systematic ex vivo MDCT scanning of human cadavers with various parameter adjustments.

The results of our study are based on clinical routine MDCT scans of the thorax and abdomen that were acquired for other purposes than diagnosing osteoporosis or estimating individual fracture risk. Thoraco-abdominal MDCT scans are among the most frequently performed radiological investigations, especially in patients with cancer for the purpose of oncological staging. Using such MDCT scans from clinical routine with the possibility of opportunistically deriving measures of bone strength could help to avoid additional dedicated DXA or quantitative CT scans, which are oftentimes additively performed. While the present study focused on the proximal femur and the herein used automated framework for multi-parametric analyses has not yet been extended to vertebral bodies, developments in the direction of broad automated opportunistic assessments of vBMD have been made at the spine [42–45]. Integrating vBMD and other determinants of bone strength from single vertebral bodies and femoral subregions may further reduce uncertainty about predictors of bone strength and fracture risk.

Limitations and perspectives

A major limitation of the present study is the monocentric design with inclusion of data from only one MDCT scanner. In clinical routine, oftentimes inhomogeneous data from different scanners from different manufacturers exist, and the herein used methods should be assessed also for data from other scanning environments. Second, MDCT scans were performed after the application of contrast agents, and related effects on HU values and, thus, on conversions to vBMD remain unadjusted. In this regard, HU measurements may not be used as an accurate proxy for actual vBMD values, and thus may not be used for defining osteoporosis or osteopenia since bone CT attenuation can vary considerably depending on factors such as the presence of intravenous contrast media [46, 47]. Specifically, there is a considerable effect of the presence of intravenously applied contrast media on HU values, which can lead to inaccurate assessment of osteoporosis [46, 47]. Bone CT attenuation is typically considerably higher in contrast-enhanced phases when compared to a non-contrast phase, and measurements in the arterial and portal phase to define osteoporosis could result in about 7 to 25% false negatives [47]. Accordingly, when accurate vBMD values should be determined from clinical routine contrast-enhanced MDCT scans, distinct correction for the presence of contrast media is warranted, which could be increasingly achieved by advanced processing algorithms based on artificial intelligence [2, 4, 42, 44, 45, 48, 49]. Third, in total we evaluated four levels for radiation dose reductions (D50 P100, D10 P100, D100 P50, and D100 P10), while finer-grained investigations with more levels would have been beneficial for determining a certain definite cutoff for both tube current lowering and sparse sampling. Specifically, given that sparse sampling with SIR enabled reductions of radiation exposure down to 10% of original imaging while still producing determinants of bone strength with clinically acceptable relative changes, also levels below 10% of the original projection data (e.g., by reading only every twentieth projection angle and deleting the remaining projections in the sinogram) could be systematically tested. In addition, combinations of simultaneously reduced lowered tube current and sparse sampling may be tested to arrive at optimal settings for

low-dose MDCT regarding spatial effects and surrogate parameters of bone strength. This could be achieved by simulations as applied in the present study, or also by ex vivo scanning of human cadavers to be able to freely and prospectively examine various parameters directly in the MDCT scanner environment. Future studies based on the results of this study may aim to systematically test further combinations of settings and to reveal respective thresholds.

Conclusion

Both virtual tube current reduction and sparse sampling with SIR for MDCT covering the proximal femur may enable low-dose examinations for opportunistically deriving image-based determinants of bone strength. However, sparse sampling may show higher potential for more drastic reductions of radiation exposure (up to 90% of original doses) when compared to tube current reductions for MDCT of the proximal femur. Based on the four simulated levels for radiation dose reductions (D50 P100, D10 P100, D100 P50, and D100 P10) of the present study, D100 P10 (i.e., 100% of the original tube current with 10% of the original projection data) with SIR may still produce determinants of bone strength with clinically acceptable relative changes, thus is the recommended setting. Yet, future studies may investigate sparse sampling also with less than 10% of the original projection data, and should also investigate combinations of reduced tube currents with reduced numbers of projections.

Supplementary Information The online version contains supplementary material available at https://doi.org/10.1007/s00198-025-07467-4.

Acknowledgements The present work was supported by the German Research Foundation (Deutsche Forschungsgemeinschaft, DFG; project 432290010: T.B. & J.S.K.), the B. Braun Foundation (project BBST-D-19-00106: N.S.), the Joachim Herz Foundation (N.S.), and R01AR080423 (JCG).

Funding Open Access funding enabled and organized by Projekt DEAL. Deutsche Forschungsgemeinschaft, 432290010, Thomas Baum and Jan S. Kirschke, B. Braun-Stiftung, BBST-D-19-00106, Nico Sollmann, Joachim Herz Stiftung, National Institute of Health, R01AR080423, Julio Carballido-Gamio.

Data availability The data that support the findings of this study are available from the corresponding author upon reasonable request.

Declarations

Ethical approval and consent to participate This retrospective single-site study was approved by the local institutional review board (registration number 5022/11-A1) and conducted in accordance with the Declaration of Helsinki. The requirement for written informed consent was waived due to the retrospective study design.

Conflict of interest None.

References

1. Compston JE, McClung MR, Leslie WD (2019) Osteoporosis Lancet 393:364–376
2. Loffler MT, Sollmann N, Mei K, Valentinitsch A, Noel PB, Kirschke JS, Baum T (2020) X-ray-based quantitative osteoporosis imaging at the spine. Osteoporos Int 31:233–250
3. Link TM, Kazakia G (2020) Update on imaging-based measurement of bone mineral density and quality. Curr Rheumatol Rep 22:13
4. Sollmann N, Kirschke JS, Kronthaler S et al (2022) Imaging of the osteoporotic spine - quantitative approaches in diagnostics and for the prediction of the individual fracture risk. Rofo 194:1088–1099
5. Praveen AD, Sollmann N, Baum T, Ferguson SJ, Benedikt H (2024) CT image-based biomarkers for opportunistic screening of osteoporotic fractures: a systematic review and meta-analysis. Osteoporos Int
6. Ammann P, Rizzoli R (2003) Bone strength and its determinants. Osteoporos Int 14(Suppl 3):S13-18
7. Fonseca H, Moreira-Goncalves D, Coriolano HJ, Duarte JA (2014) Bone quality: the determinants of bone strength and fragility. Sports Med 44:37–53
8. Friedman AW (2006) Important determinants of bone strength: beyond bone mineral density. J Clin Rheumatol 12:70–77
9. Kopperdahl DL, Aspelund T, Hoffmann PF, Sigurdsson S, Siggeirsdottir K, Harris TB, Gudnason V, Keaveny TM (2014) Assessment of incident spine and hip fractures in women and men using finite element analysis of CT scans. J Bone Miner Res 29:570–580
10. Carballido-Gamio J, Bonaretti S, Saeed I, Harnish R, Recker R, Burghardt AJ, Keyak JH, Harris T, Khosla S, Lang TF (2015) Automatic multi-parametric quantification of the proximal femur with quantitative computed tomography. Quant Imaging Med Surg 5:552–568
11. Carballido-Gamio J, Yu A, Wang L, Su Y, Burghardt AJ, Lang TF, Cheng X (2019) Hip fracture discrimination based on statistical multi-parametric modeling (SMPM). Ann Biomed Eng 47:2199–2212
12. Poole KE, Treece GM, Mayhew PM, Vaculik J, Dungl P, Horak M, Stepan JJ, Gee AH (2012) Cortical thickness mapping to identify focal osteoporosis in patients with hip fracture. PLoS ONE 7:e38466
13. Carballido-Gamio J, Harnish R, Saeed I et al (2013) Proximal femoral density distribution and structure in relation to age and hip fracture risk in women. J Bone Miner Res 28:537–546
14. Carballido-Gamio J, Harnish R, Saeed I et al (2013) Structural patterns of the proximal femur in relation to age and hip fracture risk in women. Bone 57:290–299

15. Baum T, Karampinos DC, Liebl H, Rummeny EJ, Waldt S, Bauer JS (2013) High-resolution bone imaging for osteoporosis diagnostics and therapy monitoring using clinical MDCT and MRI. Curr Med Chem 20:4844–4852
16. Dieckmeyer M, Sollmann N, Kupfer K, Loffler MT, Paprottka KJ, Kirschke JS, Baum T (2022) Computed tomography of the spine : systematic review on acquisition and reconstruction techniques to reduce radiation dose. Clin Neuroradiol
17. Costello JE, Cecava ND, Tucker JE, Bau JL (2013) CT radiation dose: current controversies and dose reduction strategies. AJR Am J Roentgenol 201:1283–1290
18. Sollmann N, Mei K, Riederer I, Schon S, Kirschke JS, Meyer B, Zimmer C, Baum T, Noel PB (2021) Low-dose MDCT of patients with spinal instrumentation using sparse sampling: impact on metal artifacts. AJR Am J Roentgenol 216:1308–1317
19. Sollmann N, Mei K, Riederer I, Probst M, Loffler MT, Kirschke JS, Noel PB, Baum T (2021) Low-dose MDCT: evaluation of the impact of systematic tube current reduction and sparse sampling on the detection of degenerative spine diseases. Eur Radiol 31:2590–2600
20. Rayudu NM, Anitha DP, Mei K et al (2020) Low-dose and sparse sampling MDCT-based femoral bone strength prediction using finite element analysis. Arch Osteoporos 15:17
21. Sollmann N, Mei K, Hedderich DM et al (2019) Multi-detector CT imaging: impact of virtual tube current reduction and sparse sampling on detection of vertebral fractures. Eur Radiol 29:3606–3616
22. Mei K, Kopp FK, Bippus R et al (2017) Is multidetector CT-based bone mineral density and quantitative bone microstructure assessment at the spine still feasible using ultra-low tube current and sparse sampling? Eur Radiol 27:5261–5271
23. Abbas S, Lee T, Shin S, Lee R, Cho S (2013) Effects of sparse sampling schemes on image quality in low-dose CT. Med Phys 40:111915
24. Willemink MJ, Noel PB (2019) The evolution of image reconstruction for CT-from filtered back projection to artificial intelligence. Eur Radiol 29:2185–2195
25. Sollmann N, Mei K, Schwaiger BJ et al (2018) Effects of virtual tube current reduction and sparse sampling on MDCT-based femoral BMD measurements. Osteoporos Int 29:2685–2692
26. Muenzel D, Koehler T, Brown K et al (2014) Validation of a low dose simulation technique for computed tomography images. PLoS ONE 9:e107843
27. Mookiah MRK, Subburaj K, Mei K, Kopp FK, Kaesmacher J, Jungmann PM, Foehr P, Noel PB, Kirschke JS, Baum T (2018) Multidetector computed tomography imaging: effect of sparse sampling and iterative reconstruction on trabecular bone microstructure. J Comput Assist Tomogr 42:441–447
28. Kim D, Ramani S, Fessler JA (2015) Combining ordered subsets and momentum for accelerated X-ray CT image reconstruction. IEEE Trans Med Imaging 34:167–178
29. Carballido-Gamio J, Posadzy M, Wu PH, Kenny K, Saeed I, Link TM, Tien PC, Krug R, Kazakia GJ (2022) People living with HIV have low trabecular bone mineral density, high bone marrow adiposity, and poor trabecular bone microarchitecture at the proximal femur. Osteoporos Int 33:1739–1753
30. Bevelacqua JJ (2010) Practical and effective ALARA. Health Phys 98(Suppl 2):S39-47
31. Castaneda S, Casas A, Gonzalez-Del-Alba A, Martinez-Diaz-Guerra G, Nogues X, Ojeda Thies C, Torregrosa Suau O, Rodriguez-Lescure A (2022) Bone loss induced by cancer treatments in breast and prostate cancer patients. Clin Transl Oncol 24:2090–2106
32. Leslie WD, Majumdar SR, Morin SN, Lix LM (2016) Change in bone mineral density is an indicator of treatment-related antifracture effect in routine clinical practice: a registry-based cohort study. Ann Intern Med 165:465–472
33. Cheung AM, Heisey R, Srighanthan J (2013) Breast cancer and osteoporosis. Curr Opin Endocrinol Diabetes Obes 20:532–538
34. Holzer G, von Skrbensky G, Holzer LA, Pichl W (2009) Hip fractures and the contribution of cortical versus trabecular bone to femoral neck strength. J Bone Miner Res 24:468–474
35. Verhulp E, van Rietbergen B, Huiskes R (2008) Load distribution in the healthy and osteoporotic human proximal femur during a fall to the side. Bone 42:30–35
36. de Bakker PM, Manske SL, Ebacher V, Oxland TR, Cripton PA, Guy P (2009) During sideways falls proximal femur fractures initiate in the superolateral cortex: evidence from high-speed video of simulated fractures. J Biomech 42:1917–1925
37. Mayhew PM, Thomas CD, Clement JG, Loveridge N, Beck TJ, Bonfield W, Burgoyne CJ, Reeve J (2005) Relation between age, femoral neck cortical stability, and hip fracture risk. Lancet 366:129–135
38. Douek PC, Boccalini S, Oei EHG, Cormode DP, Pourmorteza A, Boussel L, Si-Mohamed SA, Budde RPJ (2023) Clinical applications of photon-counting CT: a review of pioneer studies and a glimpse into the future. Radiology 309:e222432
39. Grunz JP, Huflage H (2024) Photon-counting detector CT applications in musculoskeletal radiology. Invest Radiol
40. Duan X, Wang J, Leng S, Schmidt B, Allmendinger T, Grant K, Flohr T, McCollough CH (2013) Electronic noise in CT detectors: impact on image noise and artifacts. AJR Am J Roentgenol 201:W626-632
41. Flohr T, Petersilka M, Henning A, Ulzheimer S, Ferda J, Schmidt B (2020) Photon-counting CT review. Phys Med 79:126–136
42. Sollmann N, Loffler MT, El Husseini M et al (2022) Automated opportunistic osteoporosis screening in routine computed tomography of the spine: comparison with dedicated quantitative CT. J Bone Miner Res 37:1287–1296
43. Loffler MT, Jacob A, Scharr A et al (2021) Automatic opportunistic osteoporosis screening in routine CT: improved prediction of patients with prevalent vertebral fractures compared to DXA. Eur Radiol 31:6069–6077
44. Ruhling S, Scharr A, Sollmann N et al (2022) Proposed diagnostic volumetric bone mineral density thresholds for osteoporosis and osteopenia at the cervicothoracic spine in correlation to the lumbar spine. Eur Radiol 32:6207–6214
45. Loffler MT, Sollmann N, Burian E, Bayat A, Aftahy K, Baum T, Meyer B, Ryang YM, Kirschke JS (2020) Opportunistic osteoporosis screening reveals low bone density in patients with screw loosening after lumbar semi-rigid instrumentation: a case-control study. Front Endocrinol (Lausanne) 11:552719
46. Giambini H, Dragomir-Daescu D, Huddleston PM, Camp JJ, An KN, Nassr A (2015) The effect of quantitative computed tomography acquisition protocols on bone mineral density estimation. J Biomech Eng 137:114502
47. Pompe E, Willemink MJ, Dijkhuis GR, Verhaar HJ, Mohamed Hoesein FA, de Jong PA (2015) Intravenous contrast injection significantly affects bone mineral density measured on CT. Eur Radiol 25:283–289
48. Ruhling S, Navarro F, Sekuboyina A, El Husseini M, Baum T, Menze B, Braren R, Zimmer C, Kirschke JS (2022) Automated detection of the contrast phase in MDCT by an artificial neural network improves the accuracy of opportunistic bone mineral density measurements. Eur Radiol 32:1465–1474
49. Ramschutz C, Sollmann N, El Husseini M, et al. (2024) Cervicothoracic volumetric bone mineral density assessed by opportunistic QCT may be a reliable marker for osteoporosis in adults. Osteoporos Int